ADVANCED FUNCTIONAL MATERIALS
www.afm-journal.de

Catalytic TiO_2 with Self-Assembled Monolayer for Highly Sensitive, Selective, and Non-Invasive Monitoring of Sweat L-Cysteine

Xiangjie Chen, Jia Zhu, Jian Shao, Taisong Pan, Guang Yao, Min Gao, Jian Yang, Rui Zhao, Libin Huang, Tao Li, Huanyu Cheng,* and Yuan Lin**

L-cysteine plays a significant role in numerous physiological processes in the human body health, and monitoring its level has important clinical implications. However, L-cysteine tests are limited to invasive blood drawing and a time-consuming laboratory process, which also fails to give real-time and continuous results. This study introduces a flexible electrochemical sensor based on a self-assembled monolayer (SAM) of 3-mercaptopropyltrimethoxysilane (MPTS) molecular receptor and catalytic titanium oxide-modified carbon cloth (MPTS/TiO_2/CC). The MPTS and TiO_2 modification serve as the artificial antibody through thiol interactions and the charge transfer layer, respectively, which is further confirmed by density function theory (DFT) calculations. The flexible L-cysteine sensor based on MPTS/TiO_2/CC shows a wide linear range of up to 500 µM and an ultra-low limit of detection of 0.046 µM. A sweat patch consisting of an electrochemical sensing unit, a laser-fabricated microfluidic channel, and a miniaturized electrochemical workstation affords real-time monitoring of L-cysteine detection in dynamic environments and reveals the strong correlation between sweat and blood L-cysteine concentrations. The introduction of molecular receptors and band alignment may offer a general way of designing sensitive, specific electrochemical sensors for point-of-care diagnosis.

1. Introduction

As a conditionally essential amino acid, the sulfur-containing L-cysteine is involved in synthesizing important substances in human bodies, including glutathione for protecting neurons from oxidative stress,[1] hydrogen sulfide (H_2S) for modulating synaptic transmission, and taurine for cardiovascular functionality.[2] It is vital to monitor L-cysteine levels in real-time from the blood,[3] urine,[4] and tissues[5] for health management, disease assessment, and precision nutrition.[6] Abnormal levels of L-cysteine are closely associated with oxidative stress, neurodegenerative diseases, and cardiovascular disorders. Recently, biomarkers in sweat and blood have been found to be closely correlated, making sweat an attractive medium for personalized health monitoring. Therefore, real-time and non-invasive monitoring of sweat L-cysteine concentration can help

X. Chen, J. Zhu, T. Pan, G. Yao, M. Gao, Y. Lin
School of Materials and Energy
University of Electronic Science and Technology of China
Chengdu 610054, China
E-mail: zhujia1990@uestc.edu.cn; linyuan@uestc.edu.cn

J. Zhu
Yangtze Delta Region Institute (Quzhou)
University of Electronics Science and Technology of China
Quzhou 324000, China

J. Shao
Department of Photoelectric Engineering
Lishui University
Lishui 323000, China

The ORCID identification number(s) for the author(s) of this article can be found under https://doi.org/10.1002/adfm.202511405

DOI: 10.1002/adfm.202511405

J. Yang
Research Center for Industries of the Future
Biomedical Engineering Program
School of Engineering
Westlake University
Hangzhou, Zhejiang 310030, China

R. Zhao, L. Huang, T. Li
Department of Gastroenterology
West China Hospital
Sichuan University
Chengdu 610041, China

H. Cheng
Department of Engineering Science and Mechanics
The Pennsylvania State University
University Park, Pennsylvania 16802, USA
E-mail: huanyu.cheng@psu.edu

Y. Lin
Medico-Engineering Cooperation on Applied Medicine Research Center
University of Electronics Science and Technology of China
Chengdu 610054, China

dynamically evaluate metabolic status, alert for early signs of chronic diseases, and offer new technological support for sports health management and personalized nutritional interventions. In body fluids, thiol-containing molecules such as glutathione (GSH) and homocysteine (Hcy) may indeed interfere with the electrochemical signal of L-cysteine due to their -SH group. However, the specificity test of L-cysteine can be obtained by controlling the oxidation potential and pH, as GSH and Hcy are inactive under acidic and neutral conditions. Methods commonly used for detecting L-cysteine include high-performance liquid chromatography (HPLC), nuclear magnetic resonance (NMR) spectroscopy, and fluorescence detection.[7] However, HPLC and NMR spectroscopy are expensive, complex, and time-consuming, whereas fluorescence detection is prone to background interference and has limited sensitivity. Most importantly, none of these methods can afford non-invasive, continuous monitoring for real-time evaluation of chronic cardiovascular diseases and neurological disorders.

Considering the trace amounts of L-cysteine in sweat with close correlation with that in other physiological fluids,[8] it is possible to explore highly sensitive, portable, and low-cost electrochemical sensors[9] for detecting L-cysteine over a broad linear range.[10] Nano catalytic materials are commonly employed to enhance electrochemical activities. However, electrochemical sensors based on single catalysts suffer from low specificity, as they are unable to selectively recognize target molecules over interfering substances. Although antibodies and aptamers exhibit excellent specificity and affinity,[11] they generally require strict synthesis, purification, and storage conditions, and are prone to denaturation or degradation in complex physiological environments, which limits their practical applications and long-term stability. Therefore, the development of chemical recognition sites with high specificity, ease of fabrication, and reusability is urgently needed to address these limitations. Thiol groups (—SH) in L-cysteine are highly reactive by forming disulfide bonds (—S—S—),[12] so the electrode surface modified with -SH as biorecognition elements could also provide selective L-cysteine detection. 3-Mercaptopropyltrimethoxysilane (MPTS), an organosilane compound containing thiol groups, can form self-assembled monolayers (SAMs) with exposed —SH on oxide substrates through a condensation process.[13]

Titanium dioxide (TiO_2) has widespread applications in electrochemical sensors owing to its outstanding electrochemical stability, high biocompatibility, and surface tunability.[14] As a seed layer for MPTS, TiO_2 can provide the resulting electrode with excellent electrochemical activity and biorecognition capability. During the growth of MPTS, the —OH on the TiO_2 surface undergoes a condensation reaction with silane to form stable covalent bonds.[15] TiO_2 has extraordinary electrocatalytic properties due to its partially d-orbit electrons, which serve as electron donors or acceptors, providing a tunable density of states near the Fermi level.[16] Therefore, TiO_2 serves as the seed layer for the growth of MPTS SAM and also as an excellent electrochemical catalyst to improve electron transfer efficiency.[17,18]

This work introduces a flexible, highly sensitive, and selective electrochemical sensor based on MPTS/TiO_2-modified carbon cloth (MPTS/TiO_2/CC) for continuous L-cysteine monitoring. The synthesis process is shown in **Figure 1**a. The in situ growth of TiO_2 film on CC, followed by the direct formation of MPTS SAM, provides a uniform coating of TiO_2 on the carbon fibers and a large number of MPTS molecules on the TiO_2 surface (Figure 1b). The sensing process of L-cysteine is shown in Figure 1c. L-cysteine diffusing to the electrode surface specifically reacts with the —SH groups of the MPTS and forms —S—S— disulfide bonds via redox reactions. Electrons generated during the reactions are transferred from MPTS to TiO_2 and subsequently collected by CC to realize electrochemical sensing. The MPTS/TiO_2/CC-based electrochemical sensor exhibits an outstanding limit of detection (LOD) of 0.046 μM toward L-cysteine, exceptional specificity, and long-term stability (>20 days).

The integration of the flexible sensor based on the MPTS/TiO_2/CC electrode with a skin-interface microfluidic unit and a miniaturized electrochemical workstation results in a system to continuously and wirelessly detect sweat L-cysteine during exercise (Figure 1d). The sweat produced during exercise was collected in the microchannel and reacted in the chamber. The collected data will be transmitted to external devices in real-time via Bluetooth or NFC for analysis and evaluation (Figure 1e). The miniaturized electrochemical workstation consists of five modules, namely the sensor interface, analog front end, data acquisition and processing module, data transmission module, and power management module. The real-time, continuous L-cysteine monitoring enabled by the flexible sweat patch not only has great clinical implications for cardiovascular and Alzheimer's disease control,[19] but also serves as a useful tool for precision nutrition to avoid medicine abuse (Figure 1f).

2. Results and Discussion

The comparison of diffraction peaks in the X-ray diffraction (XRD) patterns of MPTS/ TiO_2/CC, TiO_2/CC, and CC (**Figure 2**a) confirms the presence of the anatase phase of TiO_2.[20] Compared with the rutile phase, the anatase phase possesses high electronic conductivity, strong catalytic activity, and a suitable band structure,[21] which collectively contribute to enhanced sensitivity and stability of the resulting L-cysteine sensors. There are no diffraction peaks from the MPTS SAM due to poor crystallinity and low content. The successful formation of the MPTS SAM is evidenced by the presence of a weak S 2p signal in the full survey X-ray photoelectron spectroscopy (XPS) spectrum of MPTS/TiO_2/CC (Figure S1a, Supporting Information). The characteristic peaks of C—O—Ti and C—O—Si observed in the deconvoluted C 1s spectrum further confirm the effective bonding between TiO_2, MPTS, and CC (Figure S1b, Supporting Information). Peaks located at 465.5 and 459.7 eV from the high-resolution spectrum of Ti 2p (Figure 2b) are related to Ti $2p_{3/2}$ and Ti $2p_{1/2}$, respectively. The deconvoluted O 1s spectrum (Figure 2c) indicates the presence of Ti—O (531.0 eV), Si—O (533.5 eV), and C—O bonds (531.6 eV). The high-resolution spectrum of S 2p (Figure 2d) shows the presence of S—H at 164.0 eV,[22] indicating well-preserved SH from MPTS SAM. The S—S at 168.9 eV can be attributed to the coupling of exposed —SH.[23] Comparisons of the Fourier Transform Infrared (FTIR) spectra of MPTS/TiO_2/CC, TiO_2/CC, and CC further confirm the formation of the MPTS SAM (Figure 2e). The broad absorption band observed at around 3727 cm^{-1} is attributed to the stretching vibration of hydroxyl groups, indicating the possible presence of surface hydroxyl groups on both TiO_2 and MPTS SAM. The strong

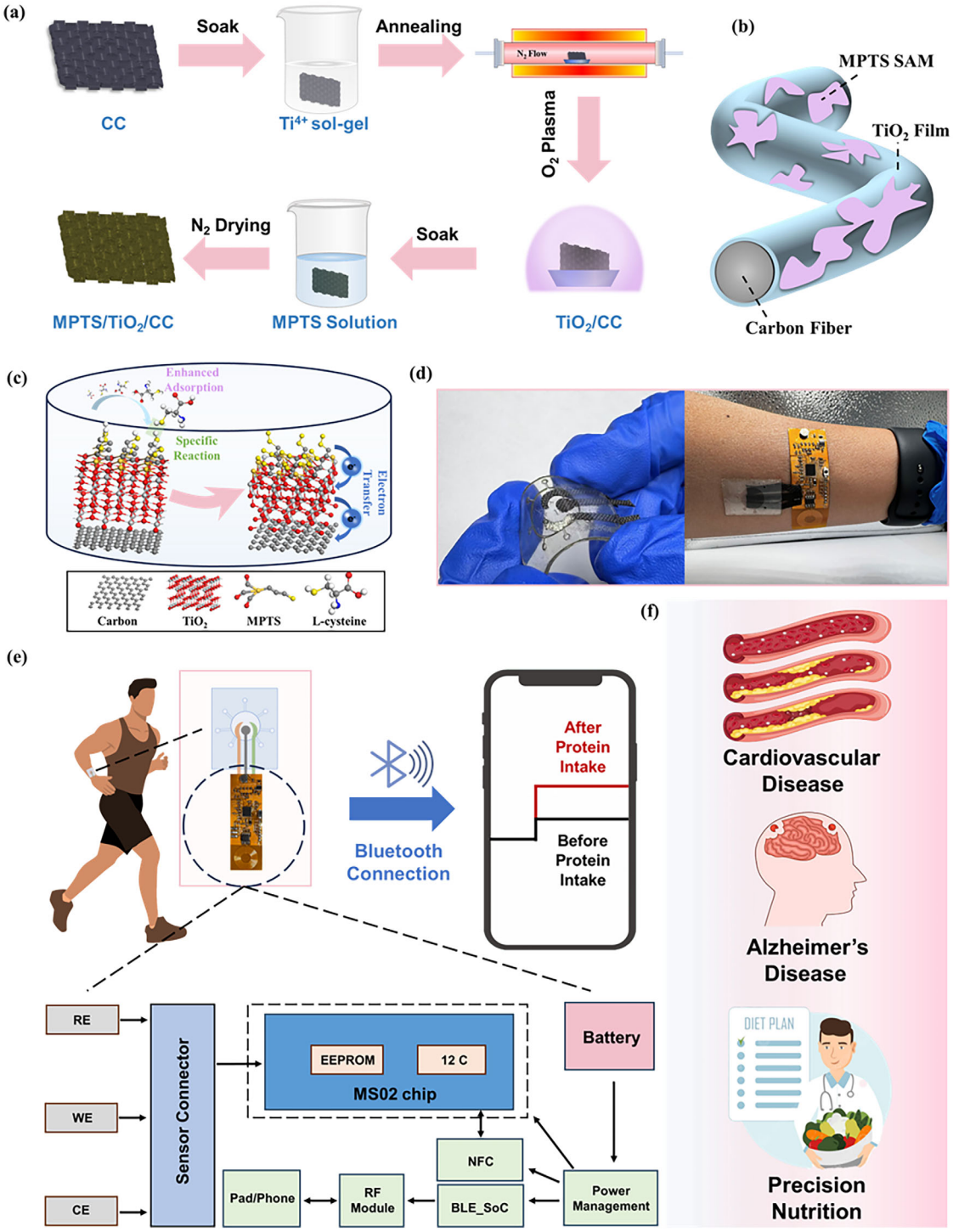

Figure 1. Schematic showing a) the preparation of 3-mercaptopropyltrimethoxysilane self-assembled monolayer on TiO_2-modified carbon cloth electrodes (MPT/TiO_2/CC) and b) the structure of the MPT/TiO_2/CC electrode, and c) its sensing mechanism toward L-cysteine. The TiO_2 layer serves as the seeding layer to coat the MPTS monolayer and facilitates the charge transfer, whereas the MPTS monolayer enables highly selective adsorption of L-cysteine for subsequent electrochemical sensing. d) Optical images of the sweat sensing module and the integrated sweat patch that was attached to human bodies. e) Block diagram of the integrated sweat patch, including an electrochemical sensor, a miniaturized, wireless electrochemical station, and an external device for display. f) Potential applications of the integrated sweat patch for cardiovascular disease and Alzheimer's disease monitoring, and precision nutrition.

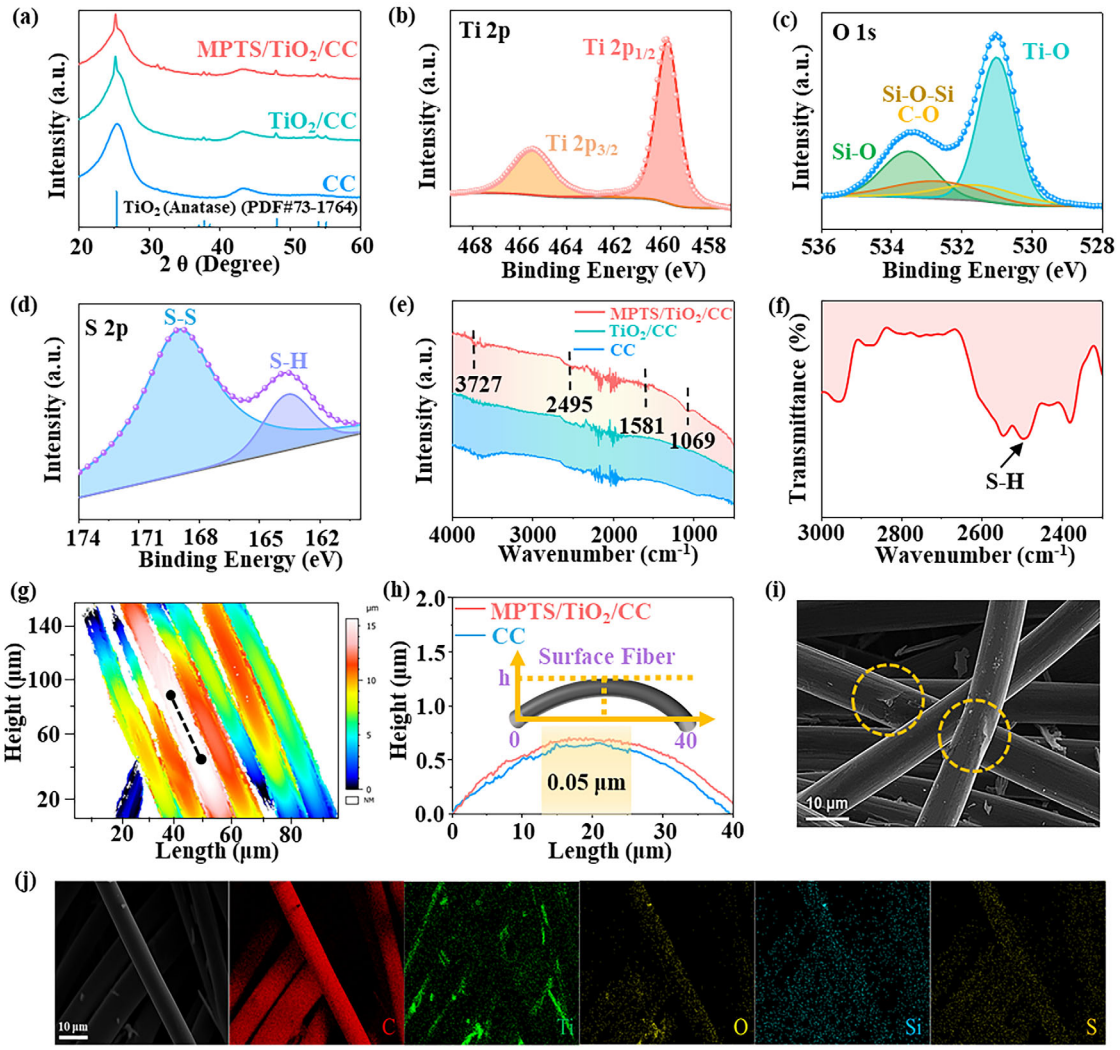

Figure 2. Material characterization of MPTS/TiO_2/CC, TiO_2/CC, and CC electrodes. a) XRD patterns of MPTS/TiO_2/CC, TiO_2/CC, and CC. XPS spectra of b) Ti 2p, c) O 1s, and d) S 2p for MPTS/TiO_2/CC. e) FTIR spectra of MPTS/TiO_2/CC, TiO_2/CC, and CC, with f) magnified FTIR spectrum of MPTS/TiO_2/CC. g) The 2D surface profile of TiO_2/CC and h) the height profile of MPTS/TiO_2/CC and CC along the fiber (the black dashed line in (g)). i) SEM image and j) EDS mapping of MPTS/TiO_2/CC.

absorption band observed at 1069 cm^{-1} originates from the characteristic asymmetric stretching vibration of Si—O—Si, suggesting the formation of siloxane bonds in the MPTS SAM. Additionally, a weak absorption band at 2495 cm^{-1} in the magnified FTIR spectrum (Figure 2f) corresponds to the stretching vibration of S-H.[24] These results collectively confirm the successful formation of the MPTS SAM on the TiO_2/CC electrode.

Although ellipsometry and atomic force microscopy (AFM) are well-established techniques for measuring film thickness, they were not employed in this study due to the fiber structure of the CC substrate. Here, confocal microscopy with the pseudo-color surface views characterizes the surface profile of the MPTS/TiO_2/CC and CC samples (Figure 2g; Figure S2, Supporting Information). The thickness of the TiO_2 film is estimated to be ≈0.05 μm from the crescent-shaped profile due to the bending of a single fiber (Figure 2h). Additionally, the surface roughness increased from 0.0193 for CC to 0.0218 μm for MPTS/TiO_2/CC calculated from the confocal microscopy images, which could provide more active sites to enhance electrochemical reactivity. The improved surface roughness is also confirmed by the rough morphology in scanning electron microscopy (SEM) images after the in situ growth of TiO_2 on CC (Figure 2i), compared to a smooth surface of CC (Figure S3, Supporting Information). The composition and distribution of S and Si on the surface of MPTS/TiO_2/CC from the Energy Dispersive Spectrometer (EDS) images (Figures 2j; Figure S4, Supporting Information) further illustrate the bonding of silane with TiO_2 and the formation of MPTS SAM.

The comparison of cyclic voltammetry (CV) and chronoamperometry curves between MPTS/TiO_2/CC, MPTS/CC, and CC highlights the important role of TiO_2 in improving the electrochemical reactivity. CV curves of the MPTS/TiO_2/CC electrode at 0.6 V toward L-cysteine reveal a distinct oxidation peak (**Figure** 3a), which can be attributed to the oxidation of

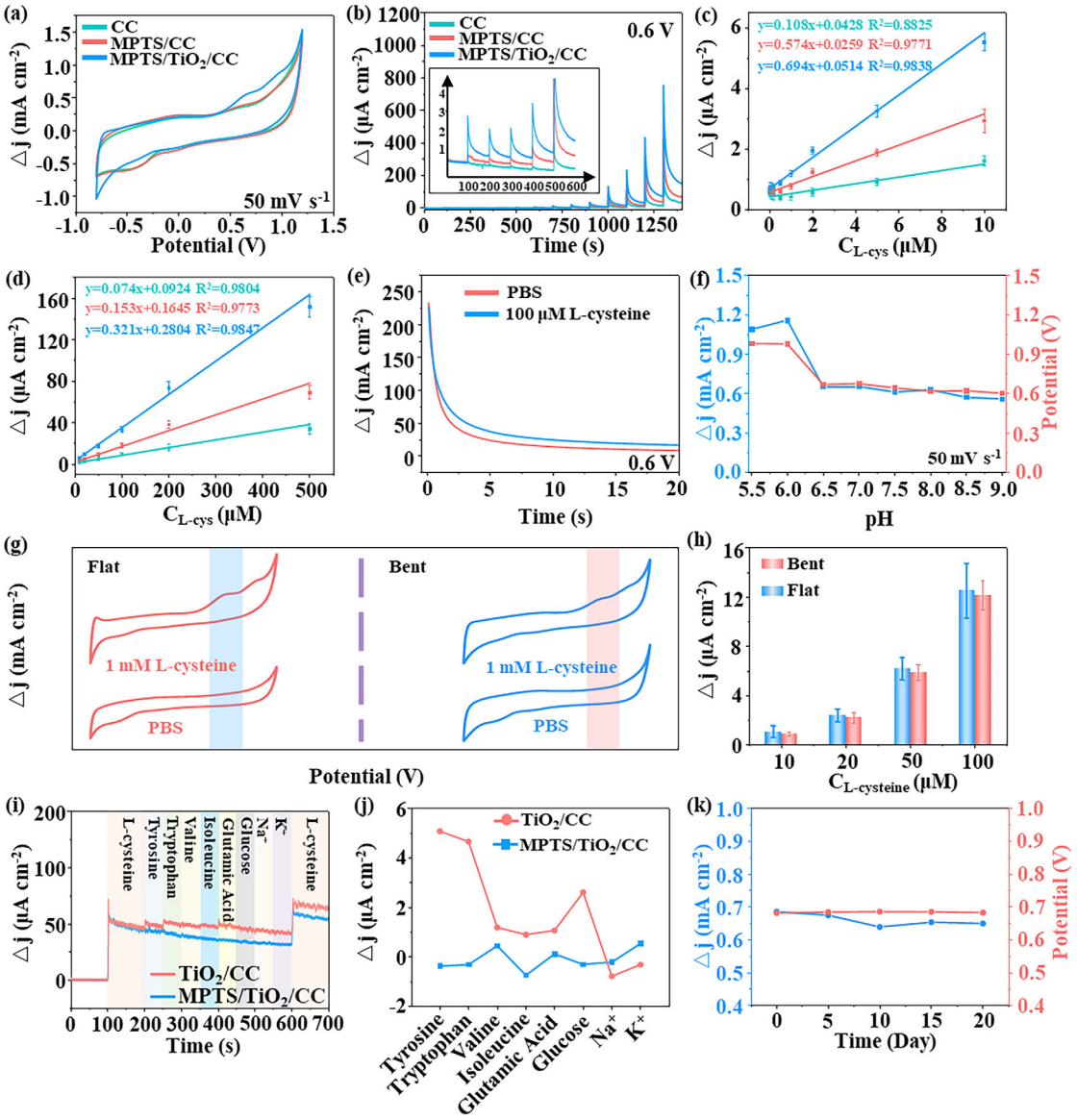

Figure 3. Electrochemical characterization of MPTS/TiO_2/CC, TiO_2/CC, and CC electrodes. a) CV curves from −0.8 to 1.2 V at 50 mV s^{-1} in 1 mM L-cysteine and b) amperometric responses from 0.05 to 500 μM at 0.6 V of MPTS/TiO_2/CC, TiO_2/CC, and CC electrodes (Inset: magnified amperometric response in the first 600 s). The corresponding calibration curves of MPTS/TiO_2/CC, TiO_2/CC, and CC electrodes with c) low (0.05–10 μM) and d) high (10–500 μM) concentrations of L-cysteine. All data points in c,d) are represented as means ± standard deviation (SD) from five samples. e) The comparison in the current response before and after adding 50 μM L-cysteine. f) The influence of pH on the peak current change (Δj) and the corresponding oxidation potential in the CV curve of MPTS/TiO_2/CC electrodes at 50 mV s^{-1}. g) Comparison in the CV curves of MPTS/TiO_2/CC electrodes before and after bending and h) the corresponding changes in Δj to different concentrations of L-cysteine. i) Amperometric response and j) corresponding current change of MTPS/TiO_2/CC and TiO_2/CC electrodes to various interferents. k) Changes in the current response and oxidation potential of MTPS/TiO_2/CC electrodes during measurements over 20 days.

L-cysteine. In comparison, the oxidation peak is barely detectable on MPTS/CC and CC electrodes due to the absence of TiO_2. This can be attributed to the efficient transfer through the unoccupied 3d orbitals of TiO_2.[16] The CV curves and chronopotentiometry curves of TiO_2/CC and CC further confirm the electrochemical catalytic effect provided by TiO_2, as shown in Figure S5 (Supporting Information). Guided by the CV curves, chronoamperometric curves of all three electrodes measured at 0.6 V exhibit instantaneously increased current density (Δj) (followed by a rapid decrease due to the reaction of L-cysteine) with the increasing L-cysteine concentration from 0.05 to 500 μM (Figure 3b). In the amperometric test, a sudden increase occurs upon the addition of L-cysteine due to the strong adsorption of L-cysteine on the electrode. During the process, a large number of electrons are released in a short time and transferred to CC, resulting in a sharp current peak. It reflects a faster rate of reaction compared with the diffusion-donimated process. Subsequently, as the L-cysteine is continuously consumed near the electrode surface, L-cysteine

from the bulk is replenished to the electrode surface through diffusion. The electrons generated during this process decrease due to the controlled amount of L-cysteine on the electrode by the diffusion process. As the diffusion reaches a steady state, the concentration gradient between the electrode surface and the bulk solution stabilizes, and the current levels off to a plateau. The linear fitting curves obtained from the steady-state current density of the chronoamperometric curves give two linear ranges with sensitivity of 0.694 and 0.321 μA cm^{-2} μM^{-1} for the L-cysteine concentration from 0.05 to 10 μM (Figure 3c) and from 10 to 500 μM (Figure 3d), respectively. The limit of detection (LOD) is defined by

$$\mathrm{LOD} = 3\sigma/S \quad (1)$$

where S and σ are the sensitivity and standard deviation, respectively.[25] The LOD is calculated to be 0.046 μM for the MPTS/TiO_2/CC electrode.

In addition, the comparison in CV curves and chronoamperometric responses between MPTS/TiO_2/CC and TiO_2/CC demonstrates the contribution of MPTS to L-cysteine detection (Figure S6, Supporting Information). The results show that the MPTS/TiO_2/CC electrode exhibits a higher current response, which can be attributed to the presence of MPTS, providing more specific adsorption sites for L-cysteine. To investigate the electron transfer and interfacial characteristics, the electrochemical impedance spectroscopy (EIS) of various electrodes was measured. The Nyquist plots show a larger interfacial charge transfer resistance of MPTS/TiO_2/CC in the high-frequency region than that of TiO_2/CC and CC electrodes (Figure S7a, Supporting Information). This is attributed to the dense MPTS SAM and TiO_2 film as a barrier, increasing the electron transfer pathway and the charge transfer resistance. On the other hand, the charge transfer resistance of the MPTS/TiO_2/CC electrode is significantly reduced after adding 0.5 mM L-cysteine, manifesting its good reactivity with L-cysteine (Figure S7b, Supporting Information).

The TiO_2 layer has dual functionalities in the MPTS/TiO_2/CC electrode: improving the electrochemical reactivity and serving as the seed layer for MPTS modifications. The MPTS SAM is immobilized on TiO_2 through a hydrolysis and condensation reaction between the silane groups of MPTS and the —OH on the surface of the TiO_2. The extraordinary electrocatalytic property of TiO_2 arising from its partially filled d-orbit electrons, abundant active sites, and oxygen vacancies and defects can greatly improve the electrochemical sensitivity of MPTS/TiO_2/CC. The choice of TiO_2 to improve electron transfer efficiency and facilitate the growth of MPTS SAM is confirmed by comparing it with two representative oxides: silicon dioxide (SiO_2) with abundant surface —OH[26] and vanadium pentoxide (V_2O_5) with excellent redox activity.[27] Both SiO_2 and V_2O_5 can serve as the seed layer for subsequent MPTS modification (Figures S8a and S9a, Supporting Information), but fail to enhance the electrochemical sensing performance of CC, as confirmed by CV (Figures S8b and S9b, Supporting Information) and chronoamperometric (Figures S8c and S9c, Supporting Information) curves of MPTS/SiO_2/CC and MPTS/V_2O_5/CC. The MPTS/SiO_2/CC electrode exhibits negligible oxidation peaks at ~0.6 V and a weak response in the chronoamperometric curve. The MPTS/V_2O_5/CC electrode shows degradation of electrochemical reactivity in CV and chronoamperometric measurements after several cycles, possibly due to the chemical instability of V_2O_5.

In CV curves at various scan rates (ν) ranging from 10 to 50 $mV{\cdot}s^{-1}$ to study the electrochemical kinetics of L-cysteine sensing (Figure S10a, Supporting Information), the nonlinear dependence of the cathodic peak current difference (Δj) on log ν is observed (Figure S10b, Supporting Information), suggesting that the sensing mechanism involves both adsorption and diffusion processes occurring simultaneously. The linear increase in Δj with ν (Figure S10c, Supporting Information) as a characteristic of the adsorption-controlled electrochemical process indicates adsorption of L-cysteine at the electrode surface before electron transfer. Meanwhile, the linear relationship between Δj and $\nu^{1/2}$ is indicative of the diffusion-controlled process (Figure S10d, Supporting Information), where the electrochemical reaction rate is limited by the transport of L-cysteine molecules from the bulk solution to the electrode surface. This diffusion-controlled behavior can be quantitatively described by the Randles-Sevcik equation:[28]

$$\Delta j = 0.4463\, n\, F\, A\, C \left(\frac{D\,\nu}{R\,T}\right)^{1/2} \quad (2)$$

where n is the number of electron transfers, F is Faraday's constant, A is the surface area of the electrode, C is the L-cysteine concentration, D is the diffusion coefficient, R is the gas constant, and T is the temperature. The diffusion coefficient of 1.01×10^{-4} cm^2 s^{-1} derived from Eq. (2) is larger than that of the other reports (Table S1, Supporting Information), indicating a faster response. The relationship between Δj and $t^{1/2}$ (Figure S11, Supporting Information) obtained from chronoamperometric measurements (Figure 3b) can be used to further confirm the aforementioned electrochemical kinetics. The linear relationship between Δj and $t^{1/2}$ within 0.5 s of adding L-cysteine indicates a rapid adsorption-controlled reaction. As the reaction proceeds, Δj decreases nonlinearly with $t^{1/2}$, reflecting a gradual transition from an adsorption- to diffusion-controlled process. The catalytic constant (K_{cat}) of MPTS/TiO_2/CC electrodes can also be determined[29] from the ratio of the stable current response of L-cysteine (I_{cat}, 100 μM) to PBS solution (I_L) (Figure 3e) as a function of the equilibrium time t (Figure S12, Supporting Information) according to: $I_{cat}/I_L = \pi^{1/2}\, K_{cat} C t^{1/2}$,[30] giving $K_{cat} = 2.01 \times 10^7$.

The measurement of biomarkers in biofluids often involves dynamic-changing pH environments.[31] Especially, the pH value profoundly affects the protonation of —SH groups of L-cysteine and its reactivity.[32] Therefore, the sensing performance of the MPTS/TiO_2/CC sensor needs to be tested at different pH values. The oxidation potential and Δj with 1 mM L-cysteine additions were measured in pH from 5.5 to 9.0 (Figure 3f; Figure S13, Supporting Information). Under an acidic environment, the amino group (—NH_2) of L-cysteine is protonated to —NH_3^+,[33] facilitating its adsorption process on the electrode surface and leading to a large current response. In addition, the carboxyl group (—COOH) of L-cysteine dissociates to —COO^- with a negatively charged molecule under alkaline conditions,[34] forming an electrostatic repulsion with TiO_2. Although the kinetics of the oxidation reaction of —SH may be enhanced under alkaline conditions, the overall reaction rate is limited by the low proton

concentration. Fortunately, the MPTS/TiO_2/CC sensor exhibits stable Δj and oxidation potential across the biological pH range, which provides significant advantages in complex biofluid monitoring.

The MPTS/TiO_2/CC sensor exhibits robust performance against bending, with negligibly small changes in Δj and oxidation peak position (Figure 3g) or over multiple (>50) cycles in the CV curves (Figure S14a, Supporting Information). The comparison in the chronoamperometric responses of electrodes before and after bending over the L-cysteine concentration from 10 to 100 μM shows a negligible change in the current density (Figure 3h; Figure S14b, Supporting Information). The specific binding between -SH in MPTS and L-cysteine, along with inhibited non-specific adsorption of other molecules,[35] enhances the selectivity of L-cysteine detection over tyrosine, tryptophan, valine, isoleucine, glutamic acid, glucose, Na^+, and K^+ (Figure 3i). Compared to the TiO_2/CC electrode responding to almost all these interfering molecules, the MPTS/TiO_2/CC electrode only exhibits a large response to L-cysteine (Figure 3j). Moreover, in further anti-interference studies (Figure S15, Supporting Information), glucose, urea, and lactic acid have little current responses due to their poor redox activity, along with a slight current response observed for electrochemically active uric acid. In contrast, a significant increase in current density is observed after the addition of L-cysteine. The active sites provided by MPTS specifically bind to L-cysteine through —SH to form —S—S—, contributing to the extraordinary selectivity of MPTS/ TiO_2/CC. The long-term chronoamperometric investigation was used to demonstrate the durability of electrodes (Figure S16, Supporting Information). After each addition of L-cysteine, the electrode maintained a long-term stable current density for ≈1000s. The reversibility of an electrode is critical for practical sensing applications, as it ensures reliable performance during repeated use and continuous monitoring. The MPTS/TiO_2/CC electrode demonstrates remarkable electrochemical stability over a period of 20 days when stored in a deoxygenated PBS solution. A negligible shift in oxidation potential and Δj is observed after 20 days (Figure 3k). Moreover, the almost unchanged calibration curves within 30 days further confirm the reversibility and stability of the MPTS/TiO_2/CC electrode (Figure S17, Supporting Information).

In addition, the comparison of the peak current density of different samples illustrates the universal preparation method of electrodes (Figure S18, Supporting Information). In summary, the MPTS/TiO_2/CC electrode with high sensitivity, low LOD, wide sensing range, excellent selectivity, and long-term stability significantly outperforms the other recently reported L-cysteine sensors (Table S2, Supporting Information).

The sensing mechanism of L-cysteine with the MPTS/TiO_2/CC electrode can be revealed by Density functional theory (DFT) calculations. After structure optimization of MPTS/TiO_2/CC, TiO_2/CC, and CC with adsorbed L-cysteine (Figure S19, Supporting Information), the differential charge density distribution was calculated to reveal the electron transfer from MPTS SAM to TiO_2 and then to CC (**Figure 4a**). The band structures of TiO_2 and MPTS/TiO_2 reveal a narrower band gap, compared to pristine TiO_2 (Figure 4b,c). Incorporating MPTS SAMs induced additional electronic states near the conduction band (CB) and valence band (VB), leading to an increased density of states (DOS) on the Fermi level. As a result, the band gap decreased from 2.286 eV (TiO_2) to 1.651 eV (MPTS/TiO_2) due to the incorporation of MPTS (Figure 4d). These additional electronic states facilitate charge transfer for improved electrochemical sensing performance.

The total density of states (TDOS) and projected density of states (PDOS) for Ti, O, Si, and S (Figure 4e–h) reveal the contributions of certain atoms to the electronic structure of the MPTS/TiO_2/CC electrode. The PDOS of Ti 3d orbitals coincide with the TDOS of Ti near the Fermi level, indicating its important role in charge transfer. The prominent peak from p orbitals of O in the valence band region also suggests the predominant contribution of O atoms to the valence band. Despite the relatively low PDOS of Si from MPTS, the modification of MPTS SAMs still contributes to DOS near the Fermi level. The vanishing PDOS of S from MPTS near the Fermi level indicates the negligible contribution of S atoms to the CB, but significantly increased DOS at the VB was observed. However, a comparison between the Ti and O DOS of MPTS/TiO_2/CC and TiO_2/CC (Figure 4e,f; Figure S20, Supporting Information) also confirms the minor influence of MPTS on the electronic structure of the CB. The adsorption energies of L-cysteine on MPTS/TiO_2/CC, TiO_2/CC, and CC electrodes are shown in Figure 4i, with values of −10.85, −1.38, and −0.32 eV, respectively. The MPTS/TiO_2/CC exhibits the highest adsorption energy for L-cysteine molecules, reaching −10.85 eV, indicating the strongest adsorption at the MPTS/TiO_2/CC interface. To summarize, theoretical calculations demonstrate that MPTS SAM and TiO_2 play an important role in the enhanced electrochemical sensing of L-cysteine.

The reaction mechanism of L-cysteine on the MPTS/TiO_2/CC electrode and the electron transfer pathway were elucidated through electrochemical characterizations and theoretical calculations.[29] As illustrated in Figure 4j, the sulfur atom in L-cysteine is initially protonated to form a positively charged —SH_2^+ intermediate, which rapidly loses a proton and generates a negatively charged thiolate anion (—S^-) (Step I). Under the applied potential, the —S^- species subsequently loses an electron to form a highly reactive sulfur radical (—S•). Simultaneously, MPTS modified on the TiO_2/CC substrate undergoes a similar electrochemical oxidation process. The —SH groups on the MPTS SAM are protonated, deprotonated, and then oxidized to generate —S• (Step II). These activated sulfur radicals on the MPTS SAM serve as highly specific chemical binding sites, enabling efficient coupling with L-cysteine molecules. In Step III, the sulfur radicals from L-cysteine and those from the MPTS SAM interact through their unpaired electrons to form stable covalent disulfide bonds (—S—S—). Additionally, as shown in Step IV, two L-cysteine molecules can dimerize on the electrode surface by forming disulfide bonds through their respective sulfur radicals. In summary, MPTS SAM provides unique binding sites for L-cysteine by forming a disulfide bond, enabling highly sensitive and selective detection.

It is well known that the efficiency of electron transfer determines the sensitivity of L-cysteine sensors. As an n-type semiconductor, TiO_2 exhibits excellent electronic conductivity, which promotes electron transfer during the electrochemical process. In addition, TiO_2 has a high electron affinity, which enables it to effectively capture electrons and promote the transport of electrons in the conduction band.[36] The electron transfer process resulting from the reactions is shown in Figure 4k. Electrons from

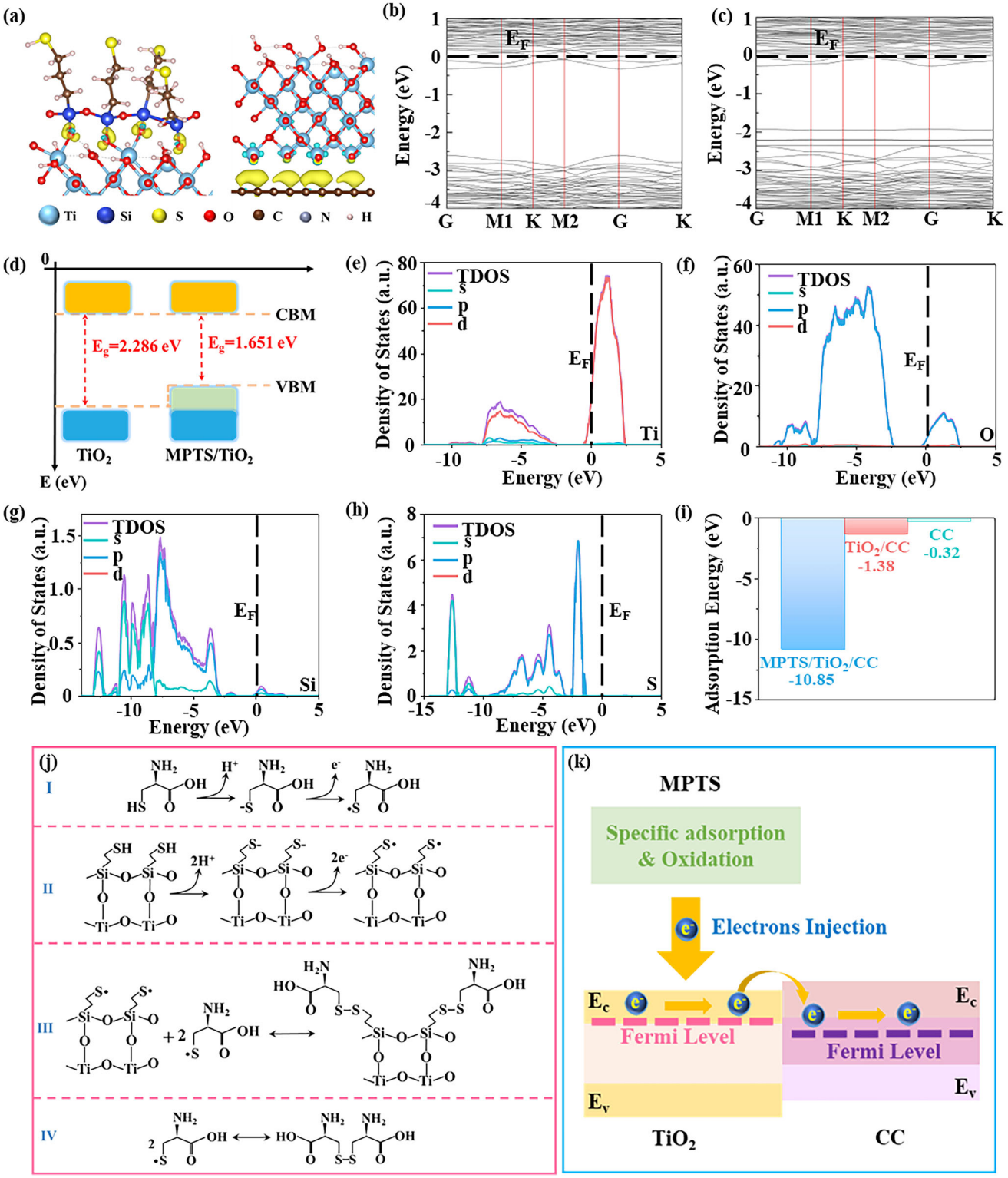

Figure 4. Theoretical simulations of the electronic structure of MPTS/TiO_2/CC electrodes. a) The differential charge density of the MPTS/TiO_2/CC electrode at the MPTS/TiO_2 (left) and TiO_2/CC (right) interfaces, with yellow and blue regions representing electron accumulation and depletion. Band structure of b) TiO_2 and c) MPTS/TiO_2, along with d) the schematics. The partial density of state of e) Ti, f) O, g) Si, and h) S in the MPTS/TiO_2/CC electrode. i) Adsorption energy of MPTS/TiO_2/CC, TiO_2/CC, and CC electrodes for L-cysteine. j) Schematic showing the reaction process between the MPTS/TiO_2/CC electrode and L-cysteine: (I) Deprotonation and oxidation of the —SH group of L-cysteine; (II) Deprotonation and oxidation of the —SH group of MPTS; (III) Oxidative coupling of MPTS with L-cysteine; and (IV) Side reactions of thiol radicals in L-cysteine. k) transfer process after redox reactions.

MPTS SAM are directly injected into the conduction band of TiO_2 and gradually migrate to the low-energy states through a series of scattering and non-radiative relaxation processes, ultimately reaching the Fermi level. Due to the difference in the Fermi levels, electrons can transfer across the interface from TiO_2 to CC, thereby promoting the conductivity of the electrode. It demonstrates that the MPTS/TiO_2/CC can provide an effective electron transfer pathway through the matching of the conduction band and Fermi level, as well as the interfacial electron transfer.

Chronoamperometry curves of MPTS/TiO_2/CC with varying concentrations of L-cysteine from 100 to 1 mM in artificial sweat, urine, and blood were performed to verify the applicability and reliability of the sensor in different body fluids (Figure S21, Supporting Information). Combining the MPTS/TiO_2/CC-based electrochemical sensor with a skin-interfaced microfluidic module yields an integrated sensing device for continuous collection and dynamic real-time analysis of sweat L-cysteine (**Figure 5a**). The flexible sweat patch consists of five laser-patterned PET or PU adhesive layers: the collection layer (CL), inflow layer (IL), electrodes layer (EL), reaction layer (RL), and outflow layer (OL). The as-fabricated integrated sweat patch can conformally attach to human skin due to the strong adhesive tape and a small overall thickness (0.6 mm) of the flexible microfluidic module (Figures 5b; Figure S22, Supporting Information). Due to the high hydrophilicity of PET, the microfluidic channel and reaction cavity were filled in 60 s with an injection rate of ≈90 µL min^{-1} and flowed out of the OL with continuous dripping (Figure 5c).

The measured results from the integrated sweat patch electrochemical method and high-performance liquid chromatography-mass spectrometry (HPLC-MS) were used to monitor the L-cysteine content in the sweat of four volunteers to verify the reliability of the electrochemistry, as shown in Figure 5d. The results reveal that the concentration of L-cysteine obtained via electrochemical methods closely matches the gold standard. The observed variations may be attributed to the inherent delay of HPLC-MS. Further integrating the sensing device with a miniaturized electrochemical workstation allows wireless, continuous measurements of sweat L-cysteine during exercise (Figure 5e), which is validated by the measurements with an electrochemical workstation (Figure 5f). The increase in current at ≈400 s (Figure 5g) corresponds to the ionic conduction between the WE and CE during the initial sweat collection. At ≈1100 s, the RL, completely immersed in sweat, initiates L-cysteine detection in the three-electrode sensor. A substantial increase in current density is observed following protein ingestion, corresponding to a rise in L-cysteine concentration from 0.066 to 0.161 µM, which can be attributed to the dietary protein intake. The concentration correlation between blood and sweat was established by monitoring L-cysteine variations using chronoamperometry (Figure 5h). The highest sweat and blood L-cysteine level was observed after protein powder intake, followed by beef, chicken breast, and water. The strong correlation confirms the feasibility of deploying the proposed flexible electrochemical sensor for real-time, non-invasive L-cysteine monitoring.

Real-time, continuous monitoring of L-cysteine levels not only has great clinical implications for people with high risks of cardiovascular and Alzheimer's diseases but also contributes to precision nutrition by avoiding medicine abuse from supplements. Previous studies indicate that the blood L-cysteine concentration of healthy individuals is in the range from 150 to 400 µM.[3] A blood L-cysteine concentration outside this range over an extended period may be associated with cardiovascular or neurological abnormalities, such as Alzheimer's disease.[37] Considering the strong correlation between blood and sweat, the integrated sweat patch combining excellent pliability and high electrochemical sensitivity, can serve as an ideal platform for these scenarios. As an example, a subject was required to wear the integrated sweat patch during various daily activities for real-time, continuous L-cysteine monitoring (Figure 5i,j). A routine workout, i.e., slow running, was adopted to stimulate sweating for L-cysteine measurements by the integrated sweat patch. The subject was involved in various daily activities, including sleeping, having a meal, and supplying nutrition, and the L-cysteine measurement was carried out afterward. The sweat L-cysteine level is relatively low (≈0.074 µM) in the morning due to the night fasting. After protein intake, the L-cysteine level elevated to 0.169 µM. L-cysteine supplements were often used for skin whitening treatments, and their proper administration is required to avoid medicine abuse that may potentially lead to cardiovascular and Alzheimer's diseases. A significantly increasing L-cysteine level up to 1.812 µM was captured by the integrated sweat patch after supplying L-cysteine. Therefore, alarms can be sent to the subject in the case of L-cysteine levels far away from the standard to avoid deterioration. Overall, the integrated sweat patch based on the MPTS/TiO_2/CC electrochemical sensor can serve as a simple yet accurate platform for real-time, continuous L-cysteine measurement, which is helpful in both disease monitoring and medicine administration.

3. Conclusion

In summary, this study showcases the DFT-guided design of a flexible electrochemical sensor based on MPTS/TiO_2/CC for the highly sensitive, selective, and long-term detection of L-cysteine in sweat. The synergistic effect of the highly catalytic TiO_2 and the specific adsorption provided by the MPTS self-assembled monolayer enables the sensor to achieve exceptional sensitivity, with response values of 0.694 and 0.321 µA cm^{-2} $µM^{-1}$ for L-cysteine concentrations ranging from 0.05 to 10 µM and 10 to 500 µM, respectively. It also demonstrates a superior limit of detection (LOD) of 0.046 µM, exceptional selectivity against other reactive amino acids, and long-term stability over 20 days, underscoring the remarkable efficacy of the SAM as artificial antibodies in biosensing. An integrated sweat patch, combining the MPTS/TiO_2/CC-based electrochemical sensor with a microfluidic module and a miniaturized electrochemical workstation, enables continuous, real-time monitoring of sweat L-cysteine levels. The strong correlation observed between sweat and blood L-cysteine levels before and after various protein intake confirms the feasibility of deploying the integrated sweat patch for health monitoring, disease assessment, and precision nutrition.

4. Experimental Section

Materials and Reagents: Tetrabutyl titanate ($C_{16}H_{36}O_4Ti$, 98%), tetraethoxysilane ($C_8H_{20}O_4Si$, 98%), vanadium pentoxide (V_2O_5, 99%), anhydrous ethanol (C_2H_5OH), Isopropanol (C_3H_8O, 99.5%) and 3-mercaptopropyltrimethoxysilane (MPTS) were purchased from Shanghai

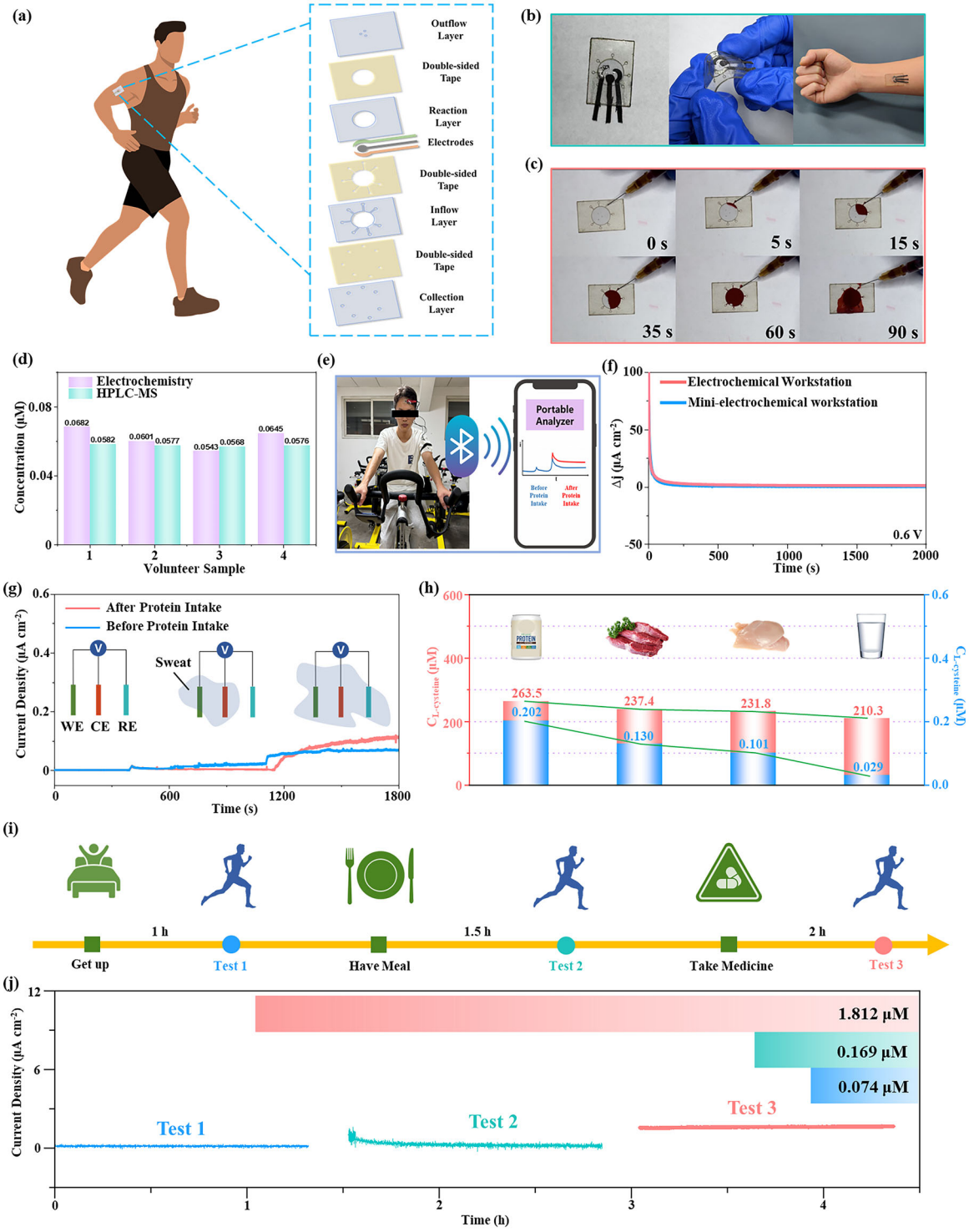

Figure 5. A wearable skin-interfaced device patch based on MPTS/TiO_2/CC electrodes for real-time monitoring of sweat L-cysteine. a) Exploded view of the flexible sweat patch sensor. Optical images of b) the as-fabricated sweat patch before and after bending and on the skin, and c) the flexible microfluidic module for fluid sampling throughout 90 s. d) Comparison of sweat L-cysteine concentrations for four volunteers measured by the electrochemical sensor and HPLC-MS. e) Experimental setup for the real-time, continuous L-cysteine monitoring by the integrated sweat patch. f) Comparison of the data sampling of the miniaturized, wireless electrochemical station and a conventional electrochemical workstation. g) Real-time current response measured by the integrated sweat patch before and after protein intake (0.6 V). h) Comparison of the measured L-cysteine concentrations in sweat and blood samples after different food intakes, including milk, beef, chicken, and water. i) Long-term and continuous monitoring of L-cysteine levels for a subject involved in various daily activities, including sleeping, doing workouts, food intake, and nutrition supplements.

Aladdin Reagent Co., Ltd. Carbon cloth (CC, HCP330N), Ag/AgCl and platinum sheet were purchased from Dongguan Kelude Experimental Equipment Technology Co., Ltd. Toluene (C_7H_8, 99.8%), hydrogen peroxide (H_2O_2, 30%) and hydrochloric acid (HCl, 37%) were purchased from Chengdu Kelong Chemical Reagent Co., Ltd. Phosphate buffer solution (PBS solution) and Polyethylene terephthalate (PET) were purchased from Chengdu Keweizhuo Technology Co., Ltd.

Synthesis of TiO_2 Sol–Gel: After adding 1.7 mL tetrabutyl titanate to 19.1 mL isopropanol during mixing, 65 µL hydrochloric acid and 90 µL deionized water were added, followed by stirring at room temperature for 6 h to obtain TiO_2 sol–gel.

Synthesis of MPTS/TiO_2/CC: First, the CC, soaked in concentrated HCl for 0.5 h to remove surface functional groups, was treated in a plasma cleaner for 300 s to prepare the hydrophilic surface. Next, CC immersed in TiO_2 sol–gel for 1 h was calcined in a tube furnace (GSL-1400X-S, Hefei Kejing Materials Technology Co., Ltd.) with N_2 atmosphere at 450 °C (heating rate of 5 °C min^{-1}) to form TiO_2/CC. After immersing the sample in the 3-mercaptopropyltrimethoxysilane (MPTS) solution (MPTS in toluene, 1:100 vol.%) for 12 h at room temperature to form a self-assembled monolayer (SAM) on the TiO_2 surface, washing with ethanol and deionized water alternatively three times was followed by drying with N_2 to obtain MPTS/TiO_2/CC.

Synthesis of MPTS/SiO_2/CC and MPTS/V_2O_5/CC: The synthesis of MPTS/SiO_2/CC started with mixing 10 mL $C_8H_{20}O_4Si$ into 13 mL deionized water, followed by adding 6.5 mL ethanol and 300 µL hydrochloric acid in sequence during the stirring process. After stirring and aging the mixture for 72 h, the HCl-treated CC was soaked in the solution for 1 h and then annealed in an N_2 atmosphere at 500 °C for 15 min to obtain MPTS/SiO_2/CC. As for MPTS/V_2O_5/CC, 0.8 g V_2O_5 powder was first dissolved in 60 mL H_2O_2 (15%) and stirred at 70 °C for 0.5 h, followed by soaking the CC in the solution for 1 h and then annealing at 300 °C for 1 h in an N_2 atmosphere.

Design and Preparation of Flexible Patch Sensors: A UV nanosecond laser cutting system (FPS21, Suzhou Delong Laser Co., Ltd., China) was used to pattern the hydrophilic PET film for assembling the microfluidic module. The Electrodes layer consists of an MPTS/TiO_2/CC working electrode (WE), an Ag/AgCl reference electrode (RE), and a CC counter electrode (CE), which are connected to a portable electrochemical analyzer (Shanghai ZB-Tech Co., Ltd., China) equipped with an integrated Bluetooth module to enable wireless data transmission to a smartphone. Each layer of the microfluidic module and reaction layer was bonded with patterned double-sided adhesive tape.

Characterizations: The electrochemical measurements in PBS were carried out with an electrochemical workstation (CHI760E, CH Instruments Inc.). Differential pulse voltammetry (DPV) was performed in the range from 0.2 to 0.8 V, whereas cyclic voltammetry (CV) curves were obtained from −0.8 to 1.2 V, with 0.6 V used for chronoamperometry. Electrochemical impedance spectroscopy (EIS) was performed in the frequency range from 0.1 to 100,000 Hz, and the collected EIS data were fitted by the Zview software. The diffraction patterns of materials in the range of 2θ from 20° to 60° were analyzed with X-ray diffraction (XRD, X'Pert Pro MPD, Netherlands). The chemical states of elements were analyzed with X-ray photoelectron spectroscopy (XPS, Thermo ESCALAB 250XI, USA). Functional groups were investigated by Fourier-transform infrared spectroscopy (FT-IR, Thermo Scientific Nicolet iS 50, USA). Confocal laser microscopy (CLSM, Leica TCS SP8, Germany) was used to analyze material surface roughness and estimate film thickness, whereas scanning electron microscopy (SEM) and energy-dispersive X-ray spectroscopy (EDS) (Zeiss Gemini 300, Germany) captured the microscopic morphology and element distribution of the material.

Density Functional Theory (DFT) Calculations: DFT calculations[38] were carried out in the VASP code[39] to reveal the interactions of L-cysteine with different substrates, by combining the Perdew-Burke-Ernzerhof (PBE) exchange and correlation functionals[40] with projector augmented wave (PAW) pseudopotentials. The energy cutoff was set to 400 eV, and k-points were generated efficiently for all calculations by following the method reported previously. The dispersion energy correction was accounted for by adopting the DFT-D3 method of Grimme with Becke-Johnson (BJ) damping.[41] MPTS/TiO_2/CC, MPTS/TiO_2, TiO_2/CC, TiO_2, and CC substrates were constructed using specific slabs. The CC slab included one layer of 4 × 4 supercells of graphene, whereas the TiO_2 slab included a 2 × 2 × 3 supercell of its (110) crystal plane. Four polymerized MPTS molecules were connected to TiO_2 through O atoms to form the MPTS/TiO_2 slab. To ensure commensurate different slabs in heterojunction and enough vacuum space in the c direction, the supercell was built into a hexagonal lattice with a = 10.3 Å and c = 40.0 Å. Each supercell was relaxed until the forces were reduced to <0.02 eV $Å^{-1}$. The band structures of MPTS/TiO_2 and TiO_2 were projected to the (110) crystal plane of the supercell. After adsorption of L-cysteine onto MPTS/TiO_2/CC, TiO_2/CC, and CC substrates, each system was relaxed using the same criterion as the substrate. The adsorption energy was calculated as:

$$E_{ad} = E_{sub} + E_{cys} - E_{sub+cys} \quad (3)$$

Supporting Information

Supporting Information is available from the Wiley Online Library or from the author.

Acknowledgements

This work is supported by the Natural Science Foundation of China under Grant Nos. 62301116, 62427806, U21A20460, and the Medico-Engineering Cooperation Funds, Fundamental Research Funds for the Central Universities, UESTC under Grant No. ZYGX2021YGLH002. H.C. acknowledges the support provided by NIH (Award No. R21EB030140), NSF (Grant Nos. 2309323, 2243979, 2319139, and 2222654), and Penn State University.

Conflict of Interest

The authors declare no conflict of interest.

Data Availability Statement

The data that support the findings of this study are available from the corresponding author upon reasonable request.

Keywords

DFT, L-cysteine, self-assembled monolayer, sweat patch, TiO_2 thin film

Received: May 7, 2025
Revised: July 30, 2025
Published online: August 16, 2025

[1] J. Duperray, R. Sergheraert, K. Chalothorn, P. Tachalerdmanee, F. Perin, *J Cosmet Dermatol* **2022**, *21*, 802.
[2] N. Shibuya, S. Koike, M. Tanaka, M. Ishigami-Yuasa, Y. Kimura, Y. Ogasawara, K. Fukui, N. Nagahara, H. Kimura, *Nat. Commun.* **2013**, *4*, 1366.
[3] S. K. Jain, D. Micinski, L. Huning, G. Kahlon, P. F. Bass, S. N. Levine, *Eur J Clin Nutr* **2014**, *68*, 1148.
[4] M. R. Majidi, K. Asadpour-Zeynali, B. Hafezi, *Microchim. Acta* **2010**, *169*, 283.
[5] M. Chroszcz-Porebska, A. Gadomska-Gajadhur, *Int. J. Mol. Sci.* **2024**, *25*, 12177.

[6] a) S. K. Jain, C. M. Stevens, J. J. Margret, S. N. Levine, *Antioxid Redox Signal* **2024**, *40*, 663; b) R. X. Liu, D. K. Song, Y. Y. Zhang, H. X. Gong, Y. C. Jin, X. S. Wang, Y. L. Jiang, Y. X. Yan, B. N. Lu, Y. M. Wu, M. Wang, X. B. Li, K. Zhang, S. B. Liu, *Neuroscience* **2024**, *555*, 213; c) N. Clemente Plaza, M. R. Garcia-Galbis, R. M. Martinez-Espinosa, *Molecules* **2018**, *23*, 575.
[7] a) S. Huang, Q. Xiao, R. Li, H. L. Guan, J. Liu, X. R. Liu, Z. K. He, Y. Liu, *Anal. Chim. Acta* **2009**, *645*, 73; b) S. Jana, *Juniper Online Journal Material Science* **2021**, *6*. c) D. Félix, D. Truzzi, A. de Godoy Netto, M. I. Soares, G. Rodrigues, J. C. Pereira, *Química Nova* **2024**, https://doi.org/10.21577/0100-4042.20240003.
[8] a) R. H. Dunstan, D. L. Sparkes, B. J. Dascombe, M. M. Macdonald, C. A. Evans, C. J. Stevens, M. J. Crompton, J. Gottfries, J. Franks, G. Murphy, R. Wood, T. K. Roberts, *PLoS One* **2016**, *11*, 0167844; b) M. M. Delgado-Povedano, M. Calderon-Santiago, F. Priego-Capote, M. D. Luque de Castro, *Talanta* **2016**, *146*, 310; c) X. Yuan, C. Li, X. Yin, Y. Yang, B. Ji, Y. Niu, L. Ren, *Biosensors (Basel)* **2023**, 13; d) C. Huang, Z. Hao, Z. Wang, H. Wang, X. Zhao, Y. Pan, *Adv. Mater. Technol.* **2022**, 7.
[9] M. H. Hassan, R. Khan, S. Andreescu, *Electrochemical Science Advances* **2021**, *2*, 2100184.
[10] S. Yang, G. Li, Y. Wang, G. Wang, L. Qu, *Microchim. Acta* **2016**, *183*, 1351.
[11] a) G. K. Ali, K. M. Omer, *Talanta* **2022**, *236*, 122878; b) Z. El-Schich, Y. Zhang, M. Feith, S. Beyer, L. Sternbaek, L. Ohlsson, M. Stollenwerk, A. G. Wingren, *BioTechniques* **2020**, *69*, 407.
[12] a) S. A. Moggach, D. R. Allan, S. J. Clark, M. J. Gutmann, S. Parsons, C. R. Pulham, L. Sawyer, *Acta Crystallogr. B* **2006**, *62*, 296; b) Y. Ma, X. Fu, Y. Shen, W. Fu, Z. Li, *Macromolecules* **2014**, *47*, 4684.
[13] a) M. Sivanandini, S. S. Dhami, B. S. Pabla, M. K. Gupta, *Procedia Mater. Sci.* **2014**, *6*, 528; b) N.-J. Huang, Q.-Q. Xia, Z.-H. Zhang, L. Zhao, G.-D. Zhang, J.-F. Gao, L.-C. Tang, *Composites, Part A* **2020**, *105*, 105797.
[14] J. Qiu, S. Zhang, H. Zhao, *Sens. Actuators, B* **2011**, *160*, 875.
[15] J. Chen, H. B. Tao, B. Liu, *Adv. Energy Mater.* **2017**, *7*, 1700886.
[16] Z. Zhang, Y. Zhu, X. Shi, B. Qi, Y. Ding, Y. Du, W. Shi, J. Zhang, J. Liu, Y. Sang, Z. Wang, L. Zhang, H. Yu, H. Zhang, B. Cai, M. Zhao, Y. Li, *Adv. Funct. Mater.* **2024**, *34*, 2316448.
[17] M. Derbali, A. Othmani, S. Kouass, F. Touati, H. Dhaouadi, *Mater. Res. Bull.* **2020**, *125*, 110771.
[18] H. Lu, J. Zhuang, Z. Ma, Y. Deng, Q. Wang, Z. Guo, S. Zhao, H. Li, *Mater. Sci. Semicond. Process.* **2019**, *97*, 21.
[19] P. A. Rasheed, R. P. Pandey, K. A. Jabbar, J. Ponraj, K. A. Mahmoud, *Anal. Methods* **2019**, *11*, 3851.
[20] X. Deng, Q. Ma, Y. Cui, X. Cheng, Q. Cheng, *Appl. Surf. Sci.* **2017**, *419*, 409.
[21] R. Katal, S. Masudy-Panah, M. Tanhaei, M. H. D. A. Farahani, H. Jiangyong, *Chem. Eng. J.* **2020**, *384*, 10.
[22] O. P. Gomes, N. F. Azevedo Neto, E. S. Bronze-Uhle, L. D. Trino, C. M. dos Santos, J. H. D. da Silva, P. N. Lisboa-Filho, *Mater. Chem. Phys.* **2019**, *223*, 32.
[23] S. P. Lin, S. Y. Huang, S. F. Chen, L. U. Vinzons, J. Y. Ciou, P. J. Wong, *ACS Appl. Mater. Interfaces* **2014**, *6*, 12071.
[24] K. K. Aswini, A. M. Vinu Mohan, V. M. Biju, *Mater Sci Eng C Mater Biol Appl* **2014**, *37*, 321.
[25] H. Evard, A. Kruve, I. Leito, *Anal. Chim. Acta* **2016**, *942*, 23.
[26] X. Wang, J. B. Xu, C. Wang, J. Du, W. Xie, *Adv. Mater.* **2011**, *23*, 2464.
[27] Y. Zhang, J. Zheng, Y. Zhao, T. Hu, Z. Gao, C. Meng, *Appl. Surf. Sci.* **2016**, *377*, 385.
[28] Z. Abdi, M. Vandichel, A. S. Sologubenko, M.-G. Willinger, J.-R. Shen, S. I. Allakhverdiev, M. M. Najafpour, *Int. J. Hydrogen Energy* **2021**, *46*, 37774.
[29] D. Geng, M. Li, X. Bo, L. Guo, *Sens. Actuators, B* **2016**, *237*, 581.
[30] G. N. Nomikos, P. Panagiotopoulou, D. I. Kondarides, X. E. Verykios, *Appl. Catal., B* **2014**, *146*, 249.
[31] J. Heikenfeld, A. Jajack, B. Feldman, S. W. Granger, S. Gaitonde, G. Begtrup, B. A. Katchman, *Nat. Biotechnol.* **2019**, *37*, 407.
[32] A. Mirzahosseini, B. Noszal, *J. Pharm. Biomed. Anal.* **2014**, *95*, 184.
[33] B. Šarac, S. Hadži, *J. Chem. Educ.* **2021**, *98*, 1001.
[34] H.-L. Gao, H. Zhang, C.-Y. Li, X.-H. Xia, *Electrochim. Acta* **2013**, *110*, 159.
[35] J. R. Winther, C. Thorpe, *Biochim. Biophys. Acta* **2014**, *1840*, 838.
[36] H. Zhu, M. Zhao, J. Zhou, W. Li, H. Wang, Z. Xu, L. Lu, L. Pei, Z. Shi, S. Yan, Z. Li, Z. Zou, *Appl. Catal., B* **2018**, *234*, 100.
[37] Y. Luo, L. Zhang, W. Liu, Y. Yu, Y. Tian, *Angew. Chem., Int. Ed.* **2015**, *54*, 14053.
[38] L. S. W. Kohn, *Phys. Rev.* **1965**, *140*, A1133.
[39] G. Kresse, J. Hafner, *Phys. Rev. B* **1993**, *47*, 558.
[40] J. P. Perdew, K. Burke, M. Ernzerhof, *Phys. Rev. Lett.* **1996**, *77*, 3865.
[41] S. Grimme, S. Ehrlich, L. Goerigk, *J. Comput. Chem.* **2011**, *32*, 1456.